1521-0103/353/2/415–423$25.00
THE JOURNAL OF PHARMACOLOGY AND EXPERIMENTAL THERAPEUTICS

http://dx.doi.org/10.1124/jpet.114.221564
J Pharmacol Exp Ther 353:415–423, May 2015

Species Differences in Hepatobiliary Disposition of Taurocholic Acid in Human and Rat Sandwich-Cultured Hepatocytes: Implications for Drug-Induced Liver Injury

Kyunghee Yang,[1] Nathan D. Pfeifer, Kathleen Köck, and Kim L. R. Brouwer

Division of Pharmacotherapy and Experimental Therapeutics, UNC Eshelman School of Pharmacy, University of North Carolina at Chapel Hill, Chapel Hill, North Carolina

Received November 29, 2014; accepted February 20, 2015

ABSTRACT

The bile salt export pump (BSEP) plays an important role in bile acid excretion. Impaired BSEP function may result in liver injury. Bile acids also undergo basolateral efflux, but the relative contributions of biliary (CL_{Bile}) versus basolateral efflux (CL_{BL}) clearance to hepatocellular bile acid excretion have not been determined. In the present study, taurocholic acid (TCA; a model bile acid) disposition was characterized in human and rat sandwich-cultured hepatocytes (SCH) combined with pharmacokinetic modeling. In human SCH, biliary excretion of TCA predominated (CL_{Bile} = 0.14 ± 0.04 ml/min per g liver; CL_{BL} = 0.042 ± 0.019 ml/min per g liver), whereas CL_{Bile} and CL_{BL} contributed approximately equally to TCA hepatocellular excretion in rat SCH (CL_{Bile} = 0.34 ± 0.07 ml/min per g liver; CL_{BL} = 0.26 ± 0.07 ml/min per g liver). Troglitazone decreased TCA uptake, CL_{Bile}, and CL_{BL}; membrane vesicle assays revealed for the first time that the major metabolite, troglitazone sulfate, was a noncompetitive inhibitor of multidrug resistance–associated protein 4, a basolateral bile acid efflux transporter. Simulations revealed that decreased CL_{Bile} led to a greater increase in hepatic TCA exposure in human than in rat SCH. A decrease in both excretory pathways (CL_{Bile} and CL_{BL}) exponentially increased hepatic TCA in both species, suggesting that 1) drugs that inhibit both pathways may have a greater risk for hepatotoxicity, and 2) impaired function of an alternate excretory pathway may predispose patients to hepatotoxicity when drugs that inhibit one pathway are administered. Simulations confirmed the protective role of uptake inhibition, suggesting that a drug's inhibitory effects on bile acid uptake also should be considered when evaluating hepatotoxic potential. Overall, the current study precisely characterized basolateral efflux of TCA, revealed species differences in hepatocellular TCA efflux pathways, and provided insights about altered hepatic bile acid exposure when multiple transport pathways are impaired.

Introduction

Bile acids are important endogenous molecules that are involved in the digestion and absorption of fats and regulation of lipid and glucose homeostasis (Hofmann, 1999a; Nguyen and Bouscarel, 2008). However, bile acids can exert toxic effects at supraphysiologic concentrations through disruption of mitochondrial ATP synthesis, necrosis, and apoptosis (Perez and Briz, 2009; Maillette de Buy Wenniger and Beuers, 2010); thus, defects in excretion may lead to hepatic accumulation of bile acids and subsequent hepatotoxicity.

Hepatic transport proteins play important roles in vectorial transport of bile acids. Sodium-taurocholate cotransporting polypeptide (NTCP) and organic anion transporting polypeptides are responsible for sodium-dependent and -independent uptake of bile acids from sinusoidal blood into hepatocytes, respectively. Bile acids in hepatocytes are excreted into bile across the canalicular membrane, predominantly via the bile salt export pump (BSEP). Consistent with the important role of BSEP in bile acid excretion, impaired BSEP function due to genetic polymorphisms has been shown to induce liver injury (e.g., progressive familial intrahepatic cholestasis type II) (Jansen et al., 1999). Also, increasing evidence suggests that inhibition of BSEP by drugs is associated with cholestatic/mixed-type drug-induced liver injury (DILI) (Morgan et al., 2010, 2013; Dawson et al., 2012; Pedersen et al., 2013).

In addition to BSEP-mediated canalicular excretion, bile acids also are transported from the hepatocyte into sinusoidal

This work was supported by the National Institutes of Health National Institute of General Medical Sciences [Grant R01-GM041935 to K.L.R.B.] and by Deutsche Forschungsgemeinschaft [Grant Ko4186/1-1 to K.K.]. The content is solely the responsibility of the authors and does not necessarily represent the official views of the National Institutes of Health.

This work was presented, in part, as a poster at the following meeting: Yang K and Brouwer KLR (2012) Pharmacokinetic modeling and simulation study to predict the impact of troglitazone (TGZ) on the hepatobiliary disposition of taurocholate (TC) in rat sandwich-cultured hepatocytes (SCH). *2012 AAPS Annual Meeting and Exposition*; 2012 Oct 14–18; Chicago, IL.

[1]Current affiliation: The Hamner-UNC Institute for Drug Safety Sciences, The Hamner Institutes for Health Sciences, Research Triangle Park, North Carolina.

dx.doi.org/10.1124/jpet.114.221564.

ABBREVIATIONS: AIC, Akaike Information Criterion; BSEP, bile salt export pump; BMI, body mass index; DHEAS, dehydroepiandrosterone sulfate; DILI, drug-induced liver injury; DMEM, Dulbecco's modified Eagle's medium; GSH, glutathione; HBSS, Hanks' balanced salt solution; MRP, multidrug resistance–associated protein; NTCP, sodium-taurocholate cotransporting polypeptide; OST, organic solute transporter; SCH, sandwich-cultured hepatocytes; TCA, taurocholic acid; TGZ, troglitazone/5-(4-[(6-hydroxy-2,5,7,8-tetramethylchroman-2-yl)methoxy]benzyl)thiazolidine-2,4-dione; TS, TGZ sulfate/5-[[4-[[3,4-dihydro-2,5,7,8-tetramethyl-6-(sulfooxy)-2*H*-1-benzopyran-2-yl]methoxy]phenyl]methyl]-2,4-thiazolidinedione; TSB, Tris-sucrose buffer.

blood via basolateral efflux transporters, including multidrug resistance–associated protein (MRP) 3, MRP4, and organic solute transporter α (OSTα)–OSTβ. Expression levels of MRP3 and MRP4 are upregulated under cholestatic conditions, suggesting that they function as a compensatory route of bile acid excretion and thereby serve as an important part of adaptive response (Akita et al., 2001; Trauner et al., 2005; Zollner et al., 2007). OSTα–OSTβ mediates basolateral efflux of bile acids from enterocytes into the portal circulation by facilitated diffusion (Ballatori et al., 2009), but the role of OSTα–OSTβ in hepatic bile acid efflux remains to be further characterized. Recently, Morgan et al. (2013) reported that prediction of DILI was improved by considering the inhibitory effect of a drug on MRP2, MRP3, and MRP4, compared with BSEP inhibition alone. In addition, studies from our laboratory demonstrated that MRP4 inhibition was associated with cholestatic/mixed DILI among BSEP noninhibitors, emphasizing the role of MRP4 in DILI (Köck et al., 2014).

DILI is one of the primary reasons for withdrawal of approved drugs from the market and a major concern during drug development (Watkins and Seeff, 2006). One prominent example is troglitazone (TGZ), the first of the thiazolidinedione class of antidiabetic drugs that was withdrawn from worldwide markets due to severe DILI. Although mechanisms of TGZ-mediated hepatotoxicity remain unclear, in vitro vesicular transport assays demonstrated that TGZ and its major metabolite, TGZ sulfate (TS), are potent BSEP inhibitors, suggesting a cholestatic component in TGZ-induced hepatotoxicity (Funk et al., 2001). TGZ also inhibits NTCP, MRP3, and MRP4 (Marion et al., 2007; Morgan et al., 2013); although TS accumulates extensively in hepatocytes (Funk et al., 2001; Lee et al., 2010), the effect of TS on basolateral efflux transporters has not been investigated.

Due to extensive biliary excretion, it generally has been accepted that the contribution of basolateral efflux to hepatocellular bile acid excretion is minimal under normal conditions. However, as proposed in the "hepatocyte hopping" theory of bilirubin glucuronides (Iusuf et al., 2012), it is plausible that bile acids may undergo extensive basolateral efflux (through MRP3 and/or MRP4) and reuptake into downstream hepatocytes (through NTCP and/or organic anion-transporting polypeptide). This would prevent saturation of biliary transporters in upstream hepatocytes and transfer bile acids to downstream hepatocytes, protecting hepatocytes from bile acid toxicity. To our knowledge, the contribution of basolateral efflux versus biliary excretion to hepatocellular bile acid disposition has not been precisely characterized.

The purpose of the present studies was to characterize taurocholic acid (TCA) hepatobiliary disposition (basolateral uptake, basolateral efflux, biliary excretion, flux from canalicular networks) in human and rat sandwich-cultured hepatocytes (SCH) using a novel uptake and efflux protocol developed by our laboratory combined with pharmacokinetic modeling (Pfeifer et al., 2013). Results from the current investigation revealed that species differences exist in cellular TCA efflux pathways in human versus rat SCH; simulations suggested differential hepatobiliary TCA disposition in human and rat SCH due to inhibitors of canalicular excretion and/or basolateral efflux. This novel finding might explain, in part, the underlying mechanisms of species differences in hepatotoxicity mediated by BSEP inhibitors. This study also investigated the effects of TGZ and its metabolites on TCA disposition in human and rat SCH, and is the first to report that TS inhibits MRP4, a basolateral bile acid efflux transporter. Last, simulations based on the constructed mechanistic models provided insights regarding altered hepatic bile acid exposure when multiple bile acid transport pathways are impaired.

Materials and Methods

All chemicals were purchased from Sigma-Aldrich (St. Louis, MO) unless otherwise stated. TGZ [5-(4-[(6-hydroxy-2,5,7,8-tetramethylchroman-2-yl)methoxy]benzyl)thiazolidine-2,4-dione] was purchased from Cayman Chemical Company (Ann Arbor, MI). TS (5-[[4-[[3,4-dihydro-2,5,7,8-tetramethyl-6-(sulfooxy)-2*H*-1-benzopyran-2-yl]methoxy]phenyl]methyl]-2,4-thiazolidinedione) was kindly provided by Daiichi-Sankyo Co., Ltd. (Tokyo, Japan). TS was also synthesized from TGZ in-house as described by Saha et al. (2010). [^{3}H]TCA (5 Ci/mmol) and [^{3}H]dehydroepiandrosterone sulfate (DHEAS; 79.5 Ci/mmol) were purchased from PerkinElmer (Waltham, MA). Dimethylsulfoxide was obtained from Fisher Scientific (Fairlawn, NJ). GIBCO brand fetal bovine serum, recombinant human insulin, and Dulbecco's modified Eagle's medium (DMEM) were purchased from Life Technologies (Carlsbad, CA). Insulin/transferrin/selenium culture supplement, BioCoat culture plates, and Matrigel extracellular matrix were purchased from BD Biosciences Discovery Labware (Bedford, MA).

Sandwich-Cultured Hepatocytes. Rat hepatocytes were isolated from male Wistar rats (234–245 g; Charles River Laboratories, Inc., Wilmington, MA) using a two-step collagenase perfusion method as previously described (LeCluyse et al., 1996). Animals had free access to water and food before surgery and were allowed to acclimate for at least 5 days. All animal procedures complied with the guidelines of the Institutional Animal Care and Use Committee (University of North Carolina, Chapel Hill, NC). Rat hepatocytes were seeded onto six-well BioCoat culture plates at a density of 1.75×10^6 cells/well in seeding medium (DMEM containing 5% fetal bovine serum, 10 μM insulin, 1 μM dexamethasone, 2 mM L-glutamine, 1% minimum essential medium nonessential amino acids, 100 units/ml of penicillin G sodium, and 100 μg/ml of streptomycin) as described previously (Swift et al., 2010). Hepatocytes were incubated for 2 hours at 37°C in a humidified incubator (95% O_2, 5% CO_2) and allowed to attach to the collagen substratum, after which time the medium was aspirated to remove unattached cells and replaced with fresh medium. The next day, cells were overlaid with BD Matrigel at a concentration of 0.25 mg/ml in ice-cold feeding medium (DMEM supplemented with 0.1 μM dexamethasone, 2 mM L-glutamine, 1% minimum essential medium nonessential amino acids, 100 units/ml of penicillin G sodium, 100 μg/ml of streptomycin, and 1% insulin/transferrin/selenium). The culture medium was changed daily until experiments were performed on day 4. Fresh human SCH, seeded onto 24-well BioCoat culture plates and overlaid with Matrigel, were purchased from Triangle Research Laboratories (Research Triangle Park, NC). Fresh human hepatocytes were obtained from two Caucasian females [31 years old, body mass index (BMI) 29.1 kg/m^2; 56 years old, BMI 22.3 kg/m^2) and one African American female (48 years old, BMI 24.9 kg/m^2). The culture medium (the same feeding medium used for rat SCH) was changed daily until experiments were performed on day 7.

Uptake and Efflux Studies in SCH. Uptake and efflux studies of TCA were performed in human and rat SCH as previously described (Pfeifer et al., 2013). In brief, on day 4 (rat) or day 7 (human) of culture, SCH were preincubated for 10 minutes in 1.5 ml/well (rat) or 0.3 ml/well (human) standard (Ca^{2+}-containing) or Ca^{2+}-free (Ca^{2+}/Mg^{2+}-free buffer containing EGTA) Hanks' balanced salt solution (HBSS). Incubating SCH in Ca^{2+}-free HBSS disrupts the tight junctions that form the bile canalicular networks (B-CLEAR technology; Qualyst Transporter Solutions, Research Triangle Park, NC). For uptake and efflux studies with TCA, SCH were treated with 1 μM [^{3}H]TCA (400 nCi/ml) in 1.5 ml/well (rat) or 0.3 ml/well (human) standard HBSS for 20 minutes at 37°C.

After the 20-minute uptake phase, buffers containing TCA were removed, cells were washed twice with 1.5 ml/well (rat) or 0.3 ml/well (human) standard or Ca^{2+}-free HBSS buffer at 37°C, and the third application of buffer was added to SCH for the 15-minute (rat) or 10-minute (human) efflux phase (Fig. 1). For determination of TGZ effects on TCA disposition, SCH were preincubated with 10 μM TGZ for 30 minutes in 1.5 ml/well (rat) or 0.3 ml/well (human) standard HBSS before 10-minute application of standard or Ca^{2+}-free HBSS. The rest of the experiment (uptake and efflux) was performed as described earlier. Preincubation was selected to minimize the inhibitory effects of TGZ and its metabolites on TCA uptake, and to allow enough time for the formation of TS, a potent BSEP inhibitor. TCA accumulation in cells + bile (standard HBSS) and cells (Ca^{2+}-free HBSS) during uptake (2, 5, 10, and 20 minutes in human SCH; 2, 5, 10, 15, and 20 minutes in rat SCH) and efflux (2, 3.5, 5, and 10 minutes in human SCH; 2, 3.5, 5, 10, and 15 minutes in rat SCH) phases was determined by terminal sampling of $n = 3$ wells at each time point. During the efflux phase, incubation buffer (standard HBSS or Ca^{2+}-free HBSS) also was collected at the end of each incubation period. Cells were washed twice in ice-cold HBSS, and were solubilized in 0.3 ml (24-well; human SCH) or 1 ml (six-well; rat SCH) 0.5% Triton X-100. Radioactivity in cell lysates and buffer samples was quantified by liquid scintillation counting (Packard TriCarb; PerkinElmer).

Pharmacokinetic Modeling. Pharmacokinetic modeling was used to evaluate the hepatobiliary disposition of TCA (control), and to determine the effects of TGZ on TCA disposition (+TGZ) in human and rat SCH. A model scheme incorporating linear parameters governing TCA disposition (Fig. 1) was fit to mass versus time data from individual SCH experiments (Fig. 2). The model fitting was performed with Phoenix WinNonlin, version 6.1 (Certara, St. Louis, MO) using the stiff estimation method and a power model to account for residual error. The following differential equations, which were developed based on the model scheme depicted in Fig. 1, were fit simultaneously to data generated in SCH in the presence of intact and disrupted bile canaliculi for each condition (human and rat; control and +TGZ):

Mass in standard HBSS buffer:

$$\frac{dX^{+}_{\text{Buffer}}}{dt} = CL_{\text{BL}} \times C^{+}_{\text{Cell}} + K_{\text{Flux}} \times X_{\text{Bile}} - CL_{\text{Uptake}} \times C^{+}_{\text{Buffer}} - K_{\text{Wash}} \times X^{+}_{\text{Buffer}}, \quad X^{+}_{\text{Buffer}}{}^{\circ} = X_{\text{dose}}$$

Mass in Ca^{2+}-free HBSS buffer:

$$\frac{dX^{-}_{\text{Buffer}}}{dt} = (CL_{\text{BL}} + CL_{\text{Bile}}) \times C^{-}_{\text{Cell}} - CL_{\text{Uptake}} \times C^{-}_{\text{Buffer}} - K_{\text{Wash}} \times X^{-}_{\text{Buffer}}, \quad X^{-}_{\text{Buffer}}{}^{\circ} = X_{\text{dose}}$$

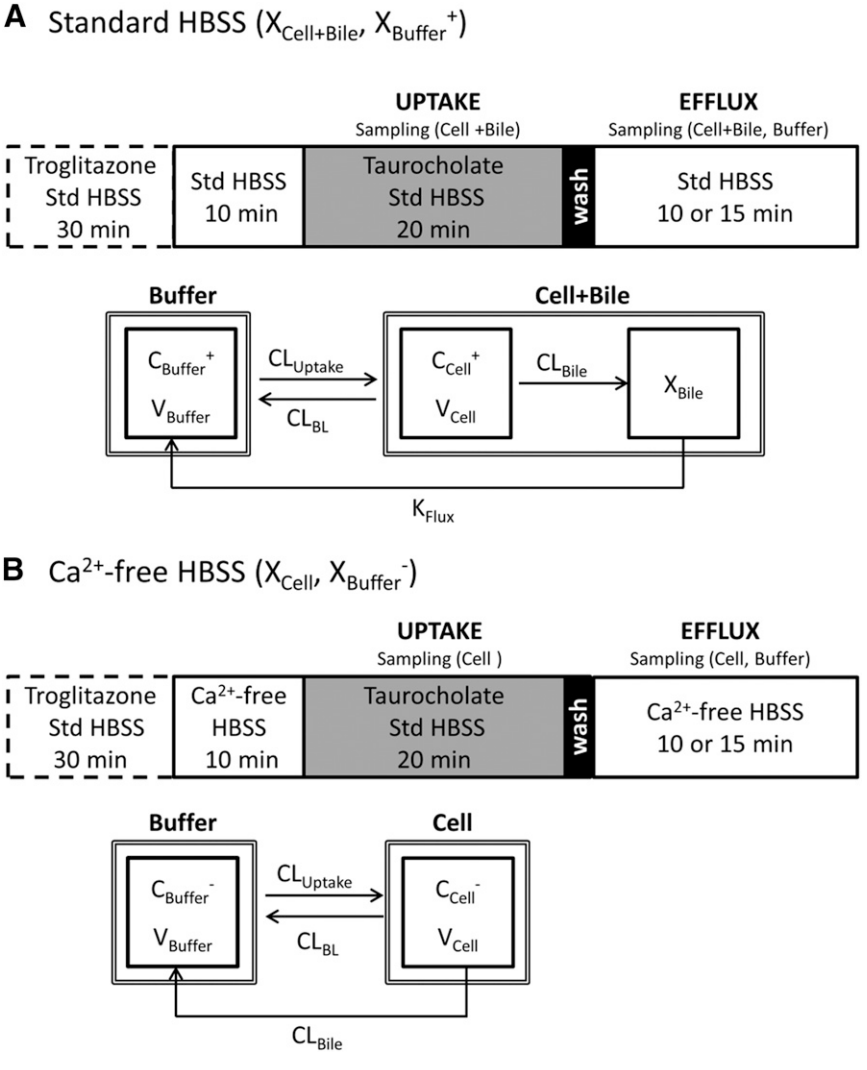

Fig. 1. Schemes depicting the uptake and efflux protocol and the mechanistic model of [^{3}H]TCA disposition in SCH. (A) Uptake and efflux studies were conducted in the presence of standard (+Ca^{2+}) Hanks' balanced salt solution (Std HBSS). Tight junctions remained sealed throughout the study period. (B) Tight junctions remained open throughout the study period by preincubating with Ca^{2+}-free HBSS, then performing an uptake phase in standard HBSS to provide relief from the removal of Ca^{2+}, followed by a brief wash and efflux in Ca^{2+}-free HBSS. In the uptake and efflux protocols, the dashed box represents preincubation with 10 μM TGZ in standard HBSS for TGZ-treated groups. Gray shading represents inclusion of the substrate, 1 μM [^{3}H]TCA, in standard HBSS during the uptake phase. Black shading represents 1-minute wash followed by 10- (human SCH) or 15-minute (rat SCH) efflux phase in standard or Ca^{2+}-free HBSS. In the model schemes, X, V, and C denote the mass of TCA, compartmental volume, and TCA concentration, respectively. Subscripts on mass, volume, and concentration terms denote the corresponding compartment in the model scheme. Superscripts represent the presence (+, intact tight junctions; cells + bile) and absence (−, modulated tight junctions; cells) of Ca^{2+} in the preincubation and efflux buffer. CL_{uptake}, CL_{BL}, and CL_{Bile} represent clearance values for uptake from buffer into hepatocytes, efflux from hepatocytes into buffer, and canalicular excretion from hepatocytes, respectively. K_{Flux} represents the first-order rate constant for flux from bile networks into buffer.

Mass in cells:

$$\frac{dX_{\text{Cell}}^{+\text{ or }-}}{dt} = CL_{\text{Uptake}} \times C_{\text{Buffer}}^{+\text{ or }-} - (CL_{\text{BL}} + CL_{\text{Bile}}) \times C_{\text{Cell}}^{+\text{ or }-}, \quad X_{\text{Cell}}^{+\text{ or }-\,\circ} = 0$$

Mass in bile (standard HBSS):

$$\frac{dX_{\text{Bile}}}{dt} = CL_{\text{Bile}} \times C_{\text{Cell}}^{+} - K_{\text{Flux}} \times X_{\text{Bile}}, \quad X_{\text{Bile}}^{\circ} = 0$$

Mass in cells+bile (standard HBSS):

$$\frac{dX_{\text{Cells + Bile}}}{dt} = \frac{dX_{\text{Bile}}}{dt} + \frac{dX_{\text{Cell}}^{+}}{dt}, \quad X_{\text{Cells + Bile}}^{\circ} = 0$$

where CL_{Bile} is the biliary clearance, CL_{BL} is the basolateral efflux clearance, CL_{Uptake} is the uptake clearance, and variables and parameters are defined as in Fig. 1, and K_{wash} was activated for 1 minute at the end of the 20-minute uptake phase and fixed at 1×10^4 min^{-1} based on simulations to eliminate the TCA dose from the buffer compartment and represent the wash step. C_{Cell} represents the intracellular concentration, calculated as $X_{\text{Cell}}/V_{\text{Cell}}$, where cellular volume (V_{Cell}) was estimated based on the protein content of each preparation, using a value of 7.4 μl/mg protein (Lee and Brouwer, 2010). C_{Buffer} represents the buffer concentration, calculated as $X_{\text{Buffer}}/V_{\text{Buffer}}$, where the buffer volume (V_{Buffer}) was constant (1.5 ml for rat SCH and 0.3 ml for human SCH). Initial parameter estimates were obtained from noncompartmental analysis of SCH data, where CL_{Uptake} was estimated from the initial (2 minutes) uptake data as follows: $CL_{\text{Uptake}} = (dX_{\text{cells+bile}}/\text{dt})/C_{\text{Buffer}}$. CL_{BL} and CL_{Bile} were estimated from efflux phase data under Ca^{2+}-free conditions, where $(CL_{\text{BL}} + CL_{\text{Bile}}) = X^{-}_{\text{Buffer,0-15min}}/\text{AUC}_{\text{cells,0-15min}}$ (area under the cellular TCA concentration versus time curve from 0 to 15 minutes, obtained using the linear trapezoidal rule). K_{Flux}, which represents the flux of substrate out of bile networks in standard HBSS conditions, was estimated initially from simulations using Berkeley-Madonna. The impact of impaired function of canalicular and/or basolateral efflux transporters on hepatic TCA exposure in human and rat SCH was simulated using the TCA model and parameter estimates (Fig. 1; Table 1); parameters representing transport-mediated efflux (CL_{BL} and CL_{Bile}) were decreased by 10-fold in isolation, or in combination, in human and rat SCH; the resulting changes in predicted cellular TCA concentrations are plotted in Fig. 4. To determine the net effect of impaired function of uptake and/or efflux (basolateral and canalicular) transporters on hepatic TCA exposure in human SCH, simulations were performed by decreasing CL_{Uptake} and CL_{Efflux} (sum of biliary and basolateral efflux clearances; $CL_{\text{BL}} + CL_{\text{Bile}}$) gradually by 10- to 100-fold in combination; it was assumed that both efflux pathways (CL_{BL} and CL_{Bile}) were impaired to the same extent. Simulated cellular TCA concentrations are presented in Fig. 5. All simulations were performed using Berkeley-Madonna version 8.3.11.

Membrane Vesicles. Human MRP4 plasmid [pcDNA3.1(−)-MRP4] was provided by Dr. Dietrich Keppler (German Cancer Research Center, Heidelberg, Germany). Human embryonic kidney 293T cell lines stably transfected with pcDNA3.1(−)-MRP4 or an empty plasmid vector (control) were established as previously described (Köck et al., 2014). Membrane vesicles were prepared from these cell lines, and transport experiments were carried out by a rapid filtration assay as described previously (Ghibellini et al., 2008). In brief, membrane vesicles (5 μg of protein) were incubated at 37°C in Tris-sucrose buffer (TSB; 50 mM Tris-HCl/250 mM sucrose) containing 10 mM $MgCl_2$, 10 mM creatine phosphate, 100 μg/ml creatine kinase, 4 mM ATP or AMP, and [^{3}H]DHEAS (0.7 μCi/ml) in the absence and presence of TS, in a volume of 50 μl. After incubation for 2 minutes, the reaction was stopped by the addition of 0.8 ml of ice-cold TSB and immediately applied to a glass fiber filter (type A/E; Pall Corp., Port Washington, NY) and washed twice with 2 ml of ice-cold TSB. Filters were mixed by vortexing in 5 ml of scintillation fluid, and radioactivity was quantified by liquid scintillation counting (Packard TriCarb). The ATP-dependent uptake of substrate was calculated by subtracting substrate uptake in the presence of AMP from substrate uptake in the presence of ATP. The MRP4-dependent uptake of substrate was calculated by subtracting ATP-dependent uptake in MRP4-overexpressing vesicles from that in control vesicles. Initially, the inhibitory effect of TS (10 μM) on MRP4-dependent transport of [^{3}H]DHEAS (2 μM) was evaluated in the presence or absence of 3 mM glutathione (GSH). Further studies were performed using concentration ranges of [^{3}H]DHEAS (0.5–20 μM) and TS (5–50 μM) in the absence of GSH to determine the inhibition constant (K_{i}). Initial estimates of K_{i} values and the type of inhibition were derived from Dixon plots of TS concentrations versus 1/velocity data. Then the kinetic parameters (K_{m}, V_{max}, and K_{i}) and type of inhibition were determined by fitting competitive, noncompetitive, and uncompetitive models to the untransformed data by nonlinear regression analysis using Phoenix WinNonlin, version 6.1. Equations used for each inhibition model are as follows:

$$\text{Competitive}: v = \frac{V_{\text{max}} \times S}{K_{\text{m}} \times \left(1 + \frac{I}{K_{\text{i}}}\right) + S}$$

$$\text{Noncompetitive}: v = \frac{V_{\text{max}} \times S}{K_{\text{m}} \times \left(1 + \frac{I}{K_{\text{i}}}\right) + S \times \left(1 + \frac{I}{K_{\text{i}}}\right)}$$

$$\text{Uncompetitive}: v = \frac{V_{\text{max}} \times S}{K_{\text{m}} + S \times \left(1 + \frac{I}{K_{\text{i}}}\right)}$$

where S represents the concentration of [^{3}H]DHEAS, I represents the concentration of TS, and V denotes the rate of [^{3}H]DHEAS transport. The best-fit model was assessed from visual inspection of the observed versus predicted data and Akaike Information Criterion (AIC). Representative data from $n = 2$ independent experiments in triplicate are presented in Fig. 3.

Data Analysis. TCA accumulation was corrected for nonspecific binding to the BioCoat plate without cells, and normalized to protein concentration measured by the BCA protein assay (Pierce Chemical, Rockford, IL). The intracellular concentration of TCA was obtained by dividing TCA accumulation (picomoles per milligram protein) by the previously reported hepatocyte volume (7.4 μl/mg protein) (Lee and Brouwer, 2010). Apparent ($CL_{\text{Bile,app}}$) and intrinsic ($CL_{\text{Bile,int}}$) biliary clearance values were calculated using B-CLEAR technology (Qualyst Transporter Solutions) based on the following equations:

$$CL_{\text{Bile,app}} = \frac{\text{Accumulation}_{\text{Cells + Bile}} - \text{Accumulation}_{\text{Cells}}}{\text{AUC}_{\text{Buffer},0-t}}$$

$$CL_{\text{Bile,int}} = \frac{\text{Accumulation}_{\text{Cells + Bile}} - \text{Accumulation}_{\text{Cells}}}{\text{AUC}_{\text{Cells},0-t}}$$

where $\text{AUC}_{\text{Buffer},0-t}$ is the area under the TCA buffer concentration versus time curve, which is the product of the initial TCA buffer concentration (1 μM) and the incubation time (t), assuming that sink conditions of TCA in the buffer are maintained (concentration changes <10% during the uptake phase). $\text{AUC}_{\text{Cell},0-t}$ is the area under the TCA cellular concentration versus time curve, which was obtained using the linear trapezoidal rule. Clearance units (microliters per minute per milligram protein) were converted to milliliters per minute per gram liver based on the protein content in liver tissue (90 and 112 mg protein/g liver for human and rat, respectively) (Sohlenius-Sternbeck, 2006). The paired Student's t test was used to compare parameters in the presence or absence of TGZ preincubation. In all cases, $P < 0.05$ was considered statistically significant. All

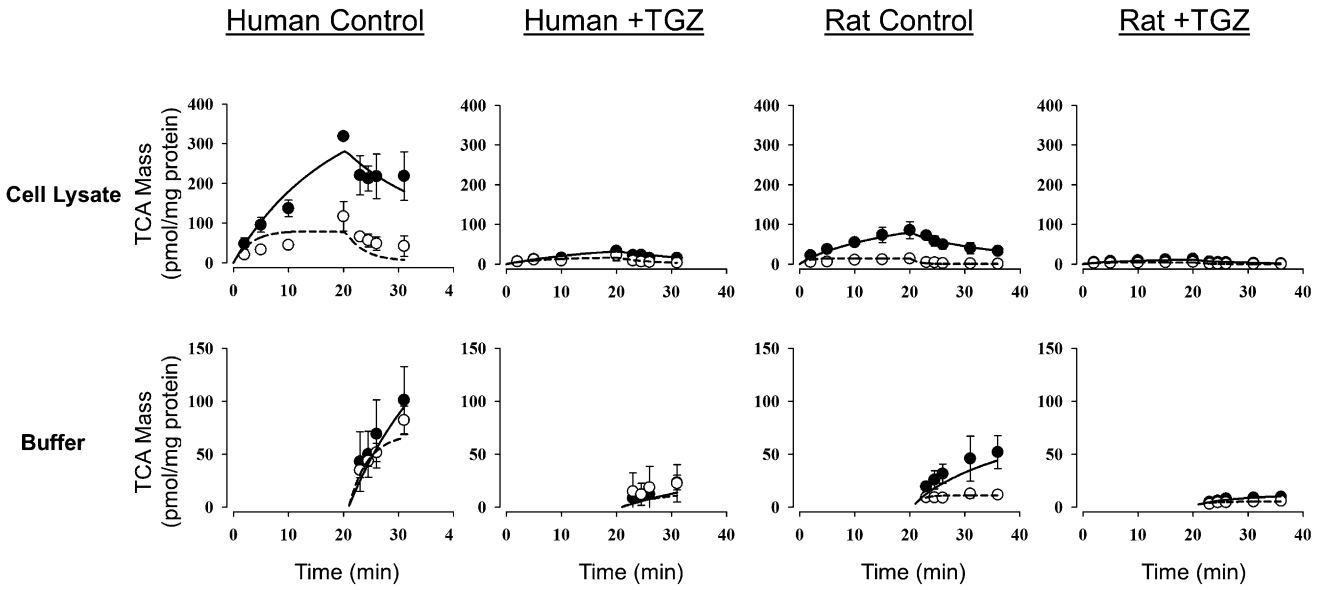

Fig. 2. [^{3}H]TCA mass versus time data in rat and human SCH in the absence (control) or presence of 10 μM TGZ preincubation. Closed symbols/solid lines represent [^{3}H]TCA in cells + bile (top) or standard HBSS (bottom), and open symbols/dashed lines represent [^{3}H]TCA in cells (top) or Ca^{2+}-free HBSS (bottom). The simulated mass-time profiles were generated from the relevant equations based on the model scheme depicted in Fig. 1, and the final parameter estimates are reported in Table 1. Data (picomoles per milligram protein) represent the mean ± S.E.M. (n = 3 SCH preparations in triplicate per group).

statistical analyses were performed using SigmaStat 3.5 (Systat Software, San Jose, CA).

Results

TCA Disposition in Human and Rat SCH with and without TGZ Preincubation. TCA uptake and efflux studies were conducted as described in Fig. 1. The mass-time profiles of TCA in cells + bile and cells (during the uptake and efflux phases) and buffer (during the efflux phase) in human and rat SCH in the absence (control) and presence (+TGZ) of TGZ preincubation are presented in Fig. 2. Under all conditions, TCA accumulation in cells + bile and cells increased during the uptake phase and decreased during the efflux phase. Appearance of TCA in the standard and Ca^{2+}-free HBSS buffer increased during the efflux phase. TGZ preincubation decreased TCA accumulation in cells + bile, cells, and the efflux into buffers in both human and rat SCH. $CL_{Bile,app}$ of TCA during the uptake phase was also significantly decreased after preincubation with TGZ compared with the control group, indicating that TGZ decreased uptake and/or biliary excretion of TCA; in human SCH, $CL_{Bile,app}$ values after 10-minute uptake (standard B-CLEAR method) in control and +TGZ groups were 1.1 ± 0.3 and 0.10 ± 0.02 ml/min per g liver, respectively (P = 0.035). The corresponding values in rat SCH were 0.48 ± 0.08 and 0.07 ± 0.01 ml/min per g liver, respectively (P = 0.008). TCA $CL_{Bile,int}$ also was significantly decreased after TGZ preincubation, suggesting that TGZ decreased TCA biliary excretion; in human SCH, $CL_{Bile,int}$ values after 10-minute uptake in control and +TGZ groups were 0.31 ± 0.07 and 0.15 ± 0.09 ml/min per g liver, respectively (P = 0.004). The corresponding values in rat SCH were 0.62 ± 0.11 and 0.22 ± 0.08 ml/min per g liver, respectively (P = 0.049).

Parameter estimates recovered from fitting differential equations (see *Materials and Methods*) based on the model scheme in Fig. 1 to TCA accumulation data from independent SCH preparations are presented in Table 1. In the absence of TGZ preincubation (control), human SCH showed greater CL_{Uptake}, slightly lower CL_{Bile}, and notably lower CL_{BL} relative to rat SCH. This is consistent with greater cellular accumulation of TCA observed in human SCH (Fig. 2). Interestingly, CL_{Bile} was about 3.3-fold greater than CL_{BL} in human SCH, whereas CL_{Bile} and CL_{BL} showed a similar contribution to the total cellular efflux of TCA in rat SCH in the absence of TGZ. In human SCH, TGZ preincubation significantly decreased CL_{Uptake} (P = 0.017); there were trends toward decreased CL_{BL} and CL_{Bile} after TGZ preincubation compared with the control groups. In rat SCH, CL_{Bile} was significantly decreased after TGZ preincubation (P = 0.017); there were trends toward decreased CL_{Uptake} and CL_{BL} after TGZ preincubation compared with the control groups. However, these differences failed to reach statistical significance due to large variability in mean differences.

Inhibitory Effects of TS on MRP4-Mediated [^{3}H]DHEAS Transport in Membrane Vesicles. The inhibitory effects of TS on MRP4, a basolateral bile acid efflux transporter, were evaluated using membrane vesicles prepared from human embryonic kidney 293T cells overexpressing MPR4 or control cells. TS (10 μM) inhibited MRP4-mediated transport of [^{3}H]DHEAS (2 μM) by 78 and 72% in the absence and presence of GSH, respectively (Fig. 3A). Inhibition of MRP4-mediated [^{3}H]DHEAS transport by TS was determined in two independent membrane vesicle studies over a range of substrate concentrations (DHEAS, 0.5–20 μM) and inhibitor concentrations (TS, 5–50 μM). In both studies, the noncompetitive inhibition model best described the inhibition data visually and generated the lowest AIC value; AIC values for competitive, noncompetitive, and uncompetitive inhibition models were

TABLE 1

Summary of recovered parameter estimates based on the model scheme depicted in Fig. 1 describing TCA disposition in human and rat SCH without (control) or with 10 μM troglitazone (+TGZ) preincubation

Human and rat SCH were treated with 1 μM [^{3}H]TCA (see Fig. 1 for details of incubation conditions), and the model was fit simultaneously to all data from each preparation. Data are presented as the mean ± S.D. of individual fits from n = 3 SCH preparations.

Conditions	CL_{Uptake}	CL_{Bile}	CL_{BL}	K_{Flux}
	ml/min per g liver			*min^{-1}*
Human SCH				
Control	2.2 ± 0.4	0.14 ± 0.04	0.042 ± 0.019	0.043 ± 0.015
+TGZ	0.23 ± 0.04*	0.084 ± 0.069	0.022 ± 0.018	0.070 ± 0.036
Rat SCH				
Control	1.2 ± 0.5	0.34 ± 0.07	0.26 ± 0.07	0.053 ± 0.015
+TGZ	0.20 ± 0.04	0.18 ± 0.05*	0.22 ± 0.06	0.077 ± 0.038

*Significantly different from control ($P < 0.05$).

632.4, 628.9, and 664.6, respectively, in the first study, and were 740.0, 738.3, and 786.0, respectively, in the second study. K_i values based on a noncompetitive inhibition model were 8.0 ± 0.70 and 8.5 ± 1.2 μM in the first and the second studies, respectively. A representative fit of the noncompetitive inhibition model to the data is presented in Fig. 3B.

Impact of Impaired Function of Canalicular versus Basolateral Efflux Transporters on Hepatic TCA Exposure. The altered hepatobiliary disposition of TCA due to impaired function of bile acid efflux transporters was simulated based on the TCA model described in this report (Fig. 1; Table 1). Simulated hepatic TCA concentrations, up to and including steady state ($C_{H,ss}$) in human and rat SCH, are shown in Fig. 4, A and B, respectively. CL_{Uptake} of TCA in rat SCH might have been underestimated compared with rats in vivo because it has been reported that TCA uptake clearance was decreased by 5-fold in rat SCH on day 4 compared with day 0 due to decreased Ntcp protein expression, whereas TCA uptake clearance remained unchanged over time in human SCH (Liu et al., 1998; Kotani et al., 2011; Tchaparian et al., 2011). To account for decreased Ntcp function over days of culture, simulations were also performed with a 5-fold higher CL_{Uptake} in rat SCH (Fig. 4C). TCA $C_{H,ss}$ was higher in human SCH (11.1 μM) compared with rat SCH (1.9 μM) (Fig. 4, A and B); this is consistent with the observed higher cellular TCA accumulation during uptake and efflux studies compared with rat SCH (Fig. 2). However, TCA $C_{H,ss}$ in rat SCH with 5-fold greater CL_{Uptake} (9.1 μM) is comparable to that in human SCH (Fig. 4, A and C). Simulations revealed that in human SCH, a 10-fold decrease in CL_{Bile} increased TCA $C_{H,ss}$ by 2.9-fold compared with control, whereas a 1.3-fold increase in TCA $C_{H,ss}$ occurred relative to control when CL_{BL} was decreased by 10-fold (Fig. 4A). Interestingly, a 10-fold decrease in both CL_{Bile} and CL_{BL} increased TCA $C_{H,ss}$ by 7.0-fold compared with control, which is a greater than proportional increase compared with inhibiting either pathway in isolation. Simulations in rat SCH revealed that TCA $C_{H,ss}$ was increased by 2.0- and 1.6-fold when CL_{Bile} and CL_{BL} were decreased by 10-fold, respectively, relative to control (Fig. 4B). TCA $C_{H,ss}$ increased by 9.3-fold relative to control when both CL_{Bile} and CL_{BL} were decreased by 10-fold; similar to human SCH simulations, the increase in $C_{H,ss}$ is greater than proportional compared with conditions in which either pathway is impaired in isolation. The same trends were observed in rat SCH when 5-fold greater CL_{Uptake} was simulated (Fig. 4C); the fold increase in TCA $C_{H,ss}$ was 1.9, 1.6, and 7.3 relative to control when CL_{Bile}, CL_{BL}, and both CL_{Bile} and CL_{BL} were decreased 10-fold, respectively.

Impact of Impaired Function of Uptake versus Efflux Transporters on Hepatic TCA Exposure in Human SCH. Hepatic bile acid concentrations are determined by both hepatic uptake and efflux processes; drugs that inhibit efflux transporters often also inhibit uptake transporters. To understand the net effects of impaired function of uptake and efflux transporters on hepatic TCA exposure, TCA $C_{H,ss}$ in human SCH was simulated based on various values of

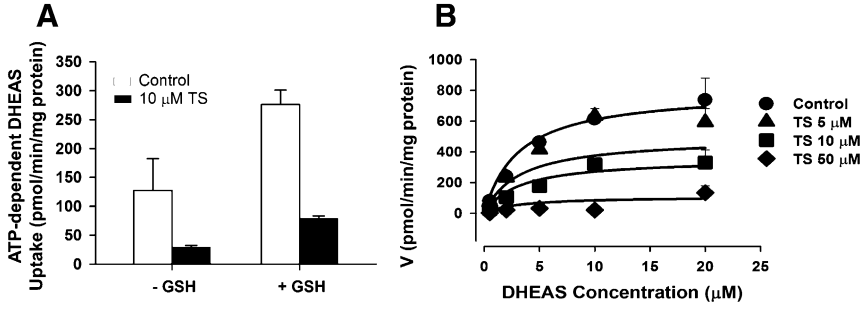

Fig. 3. Inhibition of MRP4-mediated transport of [^{3}H]DHEAS by TS in membrane vesicles from MRP4-overexpressing and control human embryonic kidney 293T cells. (A) Effect of GSH (3 mM) on MRP4-mediated transport of 2 μM [^{3}H]DHEAS and inhibition by 10 μM TS. (B) Effect of increasing concentrations of TS (0, 5, 10, and 50 μM) on MRP4-mediated [^{3}H]DHEAS (2 minutes, 0.5–20 μM) transport in the absence of GSH. Each point represents the mean ± S.D. A noncompetitive inhibition model best described the data. Lines represent model fits based on the noncompetitive inhibition model. Representative plots from n = 2 independent studies are presented. The estimated K_i values based on a noncompetitive inhibition model were 8.0 ± 0.7 and 8.5 ± 1.2 μM from each study.

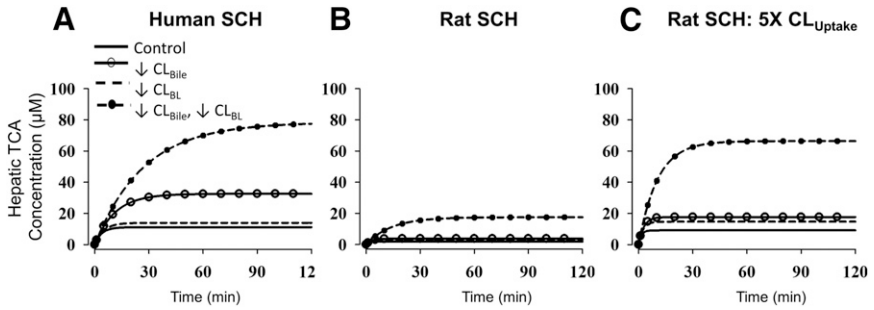

Fig. 4. Simulations depicting the impact of impaired function of canalicular and/or basolateral efflux transporters on hepatic TCA exposure. Cellular TCA concentrations in human and rat SCH were simulated based on the TCA model scheme depicted in Fig. 1 and parameter estimates (Table 1) for human SCH (A), rat SCH (B), and rat SCH where CL_{Uptake} was 5× the value listed in Table 1 (C). Parameters representing transport-mediated efflux (CL_{BL} and CL_{Bile}) were decreased by 10-fold in isolation, or in combination, to represent impaired function of canalicular efflux transporters (solid line with open circle), basolateral efflux transporters (dashed line), and both pathways (dashed line with closed circle). Simulations were performed for 200 minutes to obtain steady-state intracellular concentrations; the time to reach steady state was longer when efflux pathways were impaired compared with control (solid line).

CL_{Uptake} and CL_{Efflux} (defined as CL_{Bile} + CL_{BL}) (Fig. 5). When CL_{Uptake} remained unchanged (for example, fractional inhibition of CL_{Uptake} = 0), TCA $C_{H,ss}$ increased exponentially as the fractional inhibition of CL_{Efflux} increased. On the other hand, $C_{H,ss}$ decreased proportionally as the fractional inhibition of CL_{Uptake} increased, when CL_{Efflux} remained unchanged (for example, fractional inhibition of CL_{Efflux} = 0). When the fractional inhibition of CL_{Uptake} and CL_{Efflux} was the same, TCA $C_{H,ss}$ remained unchanged (fold change = 1). If the fractional inhibition of CL_{Uptake} was greater than the fractional inhibition of CL_{Efflux}, then TCA $C_{H,ss}$ was decreased (fold change < 1). If the fractional inhibition of CL_{Uptake} was less than the fractional inhibition of CL_{Efflux}, then the fold change in TCA $C_{H,ss}$ was greater than 1; TCA $C_{H,ss}$ increased exponentially with increasing fractional inhibition of CL_{Efflux}, but the fold change in TCA $C_{H,ss}$ decreased with increasing fractional inhibition of CL_{Uptake}. Notably, a greater than 10-fold increase in TCA $C_{H,ss}$ was observed only when the fractional inhibition of CL_{Uptake} was less than 0.6.

Discussion

The present study determined the hepatobiliary disposition of TCA in human and rat SCH using a novel uptake and efflux protocol recently developed in our laboratory combined with pharmacokinetic modeling (Pfeifer et al., 2013). The results demonstrated that species differences exist in the hepatocellular excretion of TCA; in human SCH, biliary excretion predominated, whereas biliary excretion and basolateral efflux contributed approximately equally to hepatocellular TCA excretion in rat SCH (Table 1). Jemnitz et al. (2010) reported that basolateral and biliary excretion contribute equally to TCA efflux in human SCH, whereas basolateral efflux was the dominant cellular efflux pathway of TCA in rat SCH. The likely reason for these discrepancies is that these investigators did not account for the TCA "flux" from the canalicular spaces into the buffer, which results from regular "pulsing" of the bile canaliculi in SCH (K_{Flux} in Fig. 1) (Pfeifer et al., 2014). Regular, ordered contraction of bile canaliculi has been reported previously in isolated couplets and cultured hepatocytes (Oshio and Phillips, 1981; Phillips et al., 1982), and has been shown to facilitate bile flow in vivo in rat liver (Watanabe et al., 1991). In the study by Jemnitz et al. (2010), basolateral efflux was evaluated by measuring TCA in standard buffer during the efflux phase. However, the amount of TCA that appeared in the buffer during the efflux phase was actually the sum of basolateral efflux and flux from the bile canalicular spaces, which led to an overestimation of basolateral efflux. To circumvent these issues and accurately estimate the relative contributions of CL_{BL}, CL_{Bile}, and K_{Flux}, pharmacokinetic modeling was used in the current study.

Troglitazone, a known hepatotoxic compound, was selected in the current study because disposition of TGZ and its derived metabolites was well characterized in human and rat SCH (Lee et al., 2010). After preincubation with TGZ, CL_{Bile} was significantly decreased (rat) or tended to decrease (human) compared with control (Table 1), consistent with reported inhibitory effects of TGZ and TS on BSEP (Funk et al., 2001; Dawson et al., 2012). Interestingly, CL_{BL} tended to decrease after TGZ preincubation compared with control,

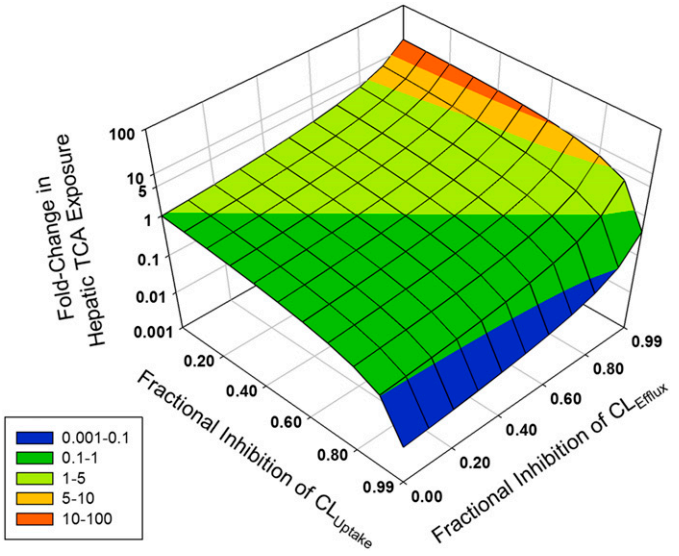

Fig. 5. Net effects of inhibition of uptake and efflux transporters on hepatic TCA exposure. Cellular TCA concentrations in human SCH were simulated as a function of decreased (10- to 100-fold) CL_{Uptake} and CL_{Efflux} (defined as CL_{BL} + CL_{Bile}); both efflux pathways (CL_{BL} and CL_{Bile}) were assumed to be impaired to the same extent. The *z*-axis represents the fold change in steady-state hepatic TCA concentrations: 10- to 100-fold (red), 5- to 10-fold (orange), 1- to 5-fold (light green), 0.1- to 1-fold (dark green), and 0.001- to 0.1-fold (blue).

suggesting that TGZ and/or TS also might inhibit basolateral efflux of TCA. TGZ has been reported to inhibit the basolateral efflux transporters MRP3 and MRP4 (Morgan et al., 2013), but hepatic TGZ concentrations are minimal, whereas TS accumulates in hepatocytes due to extensive hepatic metabolism of TGZ (Funk et al., 2001; Lee et al., 2010). Thus, inhibitory effects of TS on MRP4-mediated transport were investigated. MRP4 was selected because TCA is transported by human MRP4, but not by human MRP3 (Akita et al., 2002; Rius et al., 2006). Since GSH is cotransported with bile acids by MRP4 (Rius et al., 2006), the inhibitory effect of TS at 10 μM was tested initially in the absence and presence of GSH. TS inhibited MRP4-mediated transport of [^{3}H]DHEAS to a similar extent regardless of GSH, suggesting that the inhibitory effects of TS on MRP4 are independent of GSH (Fig. 3A). Further studies were performed in the absence of GSH, and revealed that TS inhibited MRP4-mediated [^{3}H]DHEAS transport by noncompetitive inhibition, with a K_i value of 8 μM (Fig. 3B).

In addition to inhibition of efflux, CL_{Uptake} of TCA was significantly decreased (human) or showed trends toward a decrease (rat) compared with control after TGZ preincubation (Table 1). Although TGZ is a potent inhibitor of NTCP/Ntcp-mediated bile acid uptake (Marion et al., 2007), TGZ concentrations in the buffer were minimal during the uptake phase because TGZ-containing buffer was removed and replaced with TGZ-free buffer during the 10-minute preincubation (standard or Ca^{2+}-free buffers) as well as the 20-minute uptake phase. These data suggest that TGZ might inhibit NTCP/Ntcp by mechanisms other than direct inhibition; further studies are needed to characterize the precise mechanism(s) of inhibition.

Preclinical animals often are less sensitive to bile acid–mediated DILI compared with humans, and thus, do not reliably predict human hepatotoxicity. Potential reasons include species differences in toxic bile acid composition, substrate and/or inhibitor specificity of bile acid transporters, and metabolism/detoxification pathways of drugs as well as bile acids (Setchell et al., 1997; Hofmann, 2004; Leslie et al., 2007; Chiang, 2009). In addition, differential inhibition of hepatocellular excretion pathways, as demonstrated in the current study, may contribute to species differences in bile acid–mediated hepatotoxicity. Simulations revealed that impaired function of canalicular and/or basolateral efflux transporters led to differential hepatobiliary disposition of TCA in human and rat SCH. In human SCH, hepatic TCA concentrations, which are relevant to hepatotoxicity, were increased 2.9-fold relative to control when canalicular transporter function was impaired, whereas impaired function of basolateral efflux transporters minimally increased hepatic TCA concentration (1.3-fold) (Fig. 4A). This was expected due to the predominant role of biliary excretion and the minor contribution of basolateral efflux to the overall hepatocellular excretion of TCA in human SCH. Interestingly, impaired function of both canalicular and basolateral efflux transporters further increased hepatic TCA concentrations by 7-fold compared with control (Fig. 4A), suggesting that basolateral efflux, despite serving as a minor route of hepatic excretion under normal conditions, plays an important role as a compensatory efflux pathway when canalicular excretion is impaired in human hepatocytes.

Expression and/or function of Ntcp has been reported to decrease over days of culture in rat SCH, whereas NTCP expression remains constant in human SCH; in rat SCH, TCA uptake clearance was decreased 5-fold on day 4 compared with day 0 (Liu et al., 1998; Kotani et al., 2011; Tchaparian et al., 2011). Thus, the CL_{Uptake} of TCA is likely underestimated in rat SCH, but not in human SCH. To account for the decreased function of Ntcp in day 4 rat SCH, simulations were performed in rat SCH with an CL_{Uptake} estimate obtained in day 4 rat SCH (1× CL_{Uptake}) as well as a 5-fold greater CL_{Uptake} (5× CL_{Uptake}). Although robust functional or quantitative proteomics data for BSEP, MRP3, and MRP4 in SCH over time do not exist, available data suggest that Bsep protein expression in rat SCH and MRP3/Mrp3 and MRP4/Mrp4 in rat and human SCH remain relatively unchanged over days of culture under our culture conditions (Swift et al., 2010; Tchaparian et al., 2011).

In both human and rat SCH, an exponential increase in hepatic TCA concentrations was only observed when the function of both efflux pathways was decreased (Fig. 5). These results are consistent with the mathematical relationship that governs fold change in cellular exposure: $1/(1 - fe)$, where fe is the total fraction excreted by all pathways (biliary or basolateral) (Zamek-Gliszczynski et al., 2009). Zamek-Gliszczynski et al. demonstrated that, if multiple excretion pathways exist, minor changes in exposure (<2-fold) are expected when a transport pathway that contributes to no more than 50% of total excretion is impaired, as noted when biliary excretion (rat) or basolateral efflux (human and rat) pathways alone are decreased in the current study. However, hepatic exposure increases exponentially in response to loss of function of transport pathways that contribute to >50% of total excretion, as noted in the current study when both biliary excretion and basolateral efflux transporters are impaired.

Bile acids undergo efficient enterohepatic recirculation; only ~5% of the bile acid pool is synthesized in hepatocytes, whereas the remaining 95% is reabsorbed from the intestinal lumen after biliary excretion and taken up into hepatocytes (Hofmann, 1999b). Therefore, in addition to canalicular and basolateral efflux transporters, hepatic bile acid exposure is also regulated by hepatic uptake transporters. Inhibition of bile acid efflux transporters by drugs is reported to be associated with cholestatic/mixed-type DILI, but often, these drugs also inhibit uptake transporters, which may exert protective effects (Leslie et al., 2007); the net effect will be determined by the relative extent (potency) of uptake inhibition versus efflux inhibition. As might be expected, simulations suggest that hepatic TCA exposure increases only when the extent of efflux inhibition exceeds that of uptake inhibition (Fig. 5). Notably, fractional inhibition of $CL_{Uptake} > 0.6$ prevents hepatic TCA exposure from increasing by more than 10-fold, thereby confirming the protective effects of uptake inhibition. Simulations in the current study were performed using a constant fractional inhibition of uptake and efflux transporters throughout the simulation, assuming steady-state drug (inhibitor) concentrations in the medium and in the cell. In reality, drug concentrations change over time. Thus, dynamic changes in inhibitor concentrations should be considered by incorporating drug disposition into the model to more accurately predict altered bile acid disposition by drugs.

In the current study, species differences in hepatic excretion of TCA in human and rat SCH were identified. In human SCH, biliary excretion predominated, whereas biliary excretion and basolateral efflux contributed approximately equally to TCA

efflux in rat SCH. As a result, the hepatic accumulation of TCA in rat SCH due to inhibition of BSEP alone might not be as extensive as that observed in human SCH. In human and rat SCH, inhibition of both excretion pathways led to exponential increases in hepatic TCA exposure, suggesting that inhibition of both excretion pathways might increase DILI liability. Alternatively, administration of a drug that inhibits one excretion pathway may predispose individuals with impaired transport function (due to disease or genetic polymorphisms) in the alternate pathway to hepatic bile acid accumulation and subsequent DILI. Simulations confirmed that uptake inhibition plays a protective role by helping minimize hepatic bile acid accumulation. This work emphasizes that the inhibitory effects of a drug on bile acid transporters mediating uptake as well as multiple efflux pathways should be considered when evaluating the hepatotoxic potential of drugs.

Acknowledgments

Phoenix WinNonlin software was generously provided to the Division of Pharmacotherapy and Experimental Therapeutics, UNC Eshelman School of Pharmacy, by Certara as a member of the Pharsight Academic Center of Excellence Program. The authors thank Daiichi-Sankyo Co., Ltd. for providing TS. The authors also thank Dr. Goto (UNC Eshelman School of Pharmacy) for synthesis of TS, and Dr. Keppler (German Cancer Research Center, Heidelberg, Germany) for providing the MRP4 expression vector [pcDNA3.1(+)-MRP4].

Authorship Contributions

Participated in research design: Yang, Pfeifer, Köck, Brouwer.

Conducted experiments: Yang, Pfeifer, Köck.

Performed data analysis: Yang, Pfeifer, Köck.

Wrote or contributed to the writing of the manuscript: Yang, Pfeifer, Köck, Brouwer.

References

Akita H, Suzuki H, Hirohashi T, Takikawa H, and Sugiyama Y (2002) Transport activity of human MRP3 expressed in Sf9 cells: comparative studies with rat MRP3. *Pharm Res* **19**:34–41.

Akita H, Suzuki H, and Sugiyama Y (2001) Sinusoidal efflux of taurocholate is enhanced in Mrp2-deficient rat liver. *Pharm Res* **18**:1119–1125.

Ballatori N, Li N, Fang F, Boyer JL, Christian WV, and Hammond CL (2009) OST alpha-OST beta: a key membrane transporter of bile acids and conjugated steroids. *Front Biosci (Landmark Ed)* **14**:2829–2844.

Chiang JY (2009) Bile acids: regulation of synthesis. *J Lipid Res* **50**:1955–1966.

Dawson S, Stahl S, Paul N, Barber J, and Kenna JG (2012) In vitro inhibition of the bile salt export pump correlates with risk of cholestatic drug-induced liver injury in humans. *Drug Metab Dispos* **40**:130–138.

Funk C, Ponelle C, Scheuermann G, and Pantze M (2001) Cholestatic potential of troglitazone as a possible factor contributing to troglitazone-induced hepatotoxicity: in vivo and in vitro interaction at the canalicular bile salt export pump (Bsep) in the rat. *Mol Pharmacol* **59**:627–635.

Ghibellini G, Leslie EM, Pollack GM, and Brouwer KLR (2008) Use of Tc-99m mebrofenin as a clinical probe to assess altered hepatobiliary transport: integration of in vitro, pharmacokinetic modeling, and simulation studies. *Pharm Res* **25**:1851–1860.

Hofmann AF (1999a) Bile Acids: The good, the bad, and the ugly. *News Physiol Sci* **14**:24–29.

Hofmann AF (1999b) The continuing importance of bile acids in liver and intestinal disease. *Arch Intern Med* **159**:2647–2658.

Hofmann AF (2004) Detoxification of lithocholic acid, a toxic bile acid: relevance to drug hepatotoxicity. *Drug Metab Rev* **36**:703–722.

Iusuf D, van de Steeg E, and Schinkel AH (2012) Hepatocyte hopping of OATP1B substrates contributes to efficient hepatic detoxification. *Clin Pharmacol Ther* **92**: 559–562.

Jansen PL, Strautnieks SS, Jacquemin E, Hadchouel M, Sokal EM, Hooiveld GJ, Koning JH, De Jager-Krikken A, Kuipers F, Stellaard F, et al. (1999) Hepatocanalicular bile salt export pump deficiency in patients with progressive familial intrahepatic cholestasis. *Gastroenterology* **117**:1370–1379.

Jemnitz K, Veres Z, and Vereczkey L (2010) Contribution of high basolateral bile salt efflux to the lack of hepatotoxicity in rat in response to drugs inducing cholestasis in human. *Toxicol Sci* **115**:80–88.

Köck K, Ferslew BC, Netterberg I, Yang K, Urban TJ, Swaan PW, Stewart PW, and Brouwer KLR (2014) Risk factors for development of cholestatic drug-induced liver injury: inhibition of hepatic basolateral bile acid transporters multidrug resistance-associated proteins 3 and 4. *Drug Metab Dispos* **42**:665–674.

Kotani N, Maeda K, Watanabe T, Hiramatsu M, Gong LK, Bi YA, Takezawa T, Kusuhara H, and Sugiyama Y (2011) Culture period-dependent changes in the uptake of transporter substrates in sandwich-cultured rat and human hepatocytes. *Drug Metab Dispos* **39**:1503–1510.

LeCluyse EL, Bullock PL, Parkinson A, and Hochman JH (1996) Cultured rat hepatocytes. *Pharm Biotechnol* **8**:121–159.

Lee JK and Brouwer KR (2010) Determination of intracellular volume of rat and human sandwich-cultured hepatocytes (Abstract ID 1595). *The Toxicologist. Supplement to Toxicological Sciences* **114**:339.

Lee JK, Marion TL, Abe K, Lim C, Pollack GM, and Brouwer KLR (2010) Hepatobiliary disposition of troglitazone and metabolites in rat and human sandwich-cultured hepatocytes: use of Monte Carlo simulations to assess the impact of changes in biliary excretion on troglitazone sulfate accumulation. *J Pharmacol Exp Ther* **332**:26–34.

Leslie EM, Watkins PB, Kim RB, and Brouwer KLR (2007) Differential inhibition of rat and human Na^+-dependent taurocholate cotransporting polypeptide (NTCP/SLC10A1) by bosentan: a mechanism for species differences in hepatotoxicity. *J Pharmacol Exp Ther* **321**:1170–1178.

Liu X, Brouwer KLR, Gan LS, Brouwer KR, Stieger B, Meier PJ, Audus KL, and LeCluyse EL (1998) Partial maintenance of taurocholate uptake by adult rat hepatocytes cultured in a collagen sandwich configuration. *Pharm Res* **15**: 1533–1539.

Maillette de Buy Wenniger L and Beuers U (2010) Bile salts and cholestasis. *Dig Liver Dis* **42**:409–418.

Marion TL, Leslie EM, and Brouwer KLR (2007) Use of sandwich-cultured hepatocytes to evaluate impaired bile acid transport as a mechanism of drug-induced hepatotoxicity. *Mol Pharm* **4**:911–918.

Morgan RE, Trauner M, van Staden CJ, Lee PH, Ramachandran B, Eschenberg M, Afshari CA, Qualls CW, Jr, Lightfoot-Dunn R, and Hamadeh HK (2010) Interference with bile salt export pump function is a susceptibility factor for human liver injury in drug development. *Toxicol Sci* **118**:485–500.

Morgan RE, van Staden CJ, Chen Y, Kalyanaraman N, Kalanzi J, Dunn RT, 2nd, Afshari CA, and Hamadeh HK (2013) A multifactorial approach to hepatobiliary transporter assessment enables improved therapeutic compound development. *Toxicol Sci* **136**:216–241.

Nguyen A and Bouscarel B (2008) Bile acids and signal transduction: role in glucose homeostasis. *Cell Signal* **20**:2180–2197.

Oshio C and Phillips MJ (1981) Contractility of bile canaliculi: implications for liver function. *Science* **212**:1041–1042.

Pedersen JM, Matsson P, Bergström CA, Hoogstraate J, Norén A, LeCluyse EL, and Artursson P (2013) Early identification of clinically relevant drug interactions with the human bile salt export pump (BSEP/ABCB11). *Toxicol Sci* **136**:328–343.

Perez MJ and Briz O (2009) Bile-acid-induced cell injury and protection. *World J Gastroenterol* **15**:1677–1689.

Pfeifer ND, Hardwick RN, and Brouwer KLR (2014) Role of hepatic efflux transporters in regulating systemic and hepatocyte exposure to xenobiotics. *Annu Rev Pharmacol Toxicol* **54**:509–535.

Pfeifer ND, Yang K, and Brouwer KLR (2013) Hepatic basolateral efflux contributes significantly to rosuvastatin disposition I: characterization of basolateral versus biliary clearance using a novel protocol in sandwich-cultured hepatocytes. *J Pharmacol Exp Ther* **347**:727–736.

Phillips MJ, Oshio C, Miyairi M, Katz H, and Smith CR (1982) A study of bile canalicular contractions in isolated hepatocytes. *Hepatology* **2**:763–768.

Rius M, Hummel-Eisenbeiss J, Hofmann AF, and Keppler D (2006) Substrate specificity of human ABCC4 (MRP4)-mediated cotransport of bile acids and reduced glutathione. *Am J Physiol Gastrointest Liver Physiol* **290**:G640–G649.

Saha S, New LS, Ho HK, Chui WK, and Chan EC (2010) Direct toxicity effects of sulfo-conjugated troglitazone on human hepatocytes. *Toxicol Lett* **195**:135–141.

Setchell KD, Rodrigues CM, Clerici C, Solinas A, Morelli A, Gartung C, and Boyer J (1997) Bile acid concentrations in human and rat liver tissue and in hepatocyte nuclei. *Gastroenterology* **112**:226–235.

Sohlenius-Sternbeck AK (2006) Determination of the hepatocellularity number for human, dog, rabbit, rat and mouse livers from protein concentration measurements. *Toxicol In Vitro* **20**:1582–1586.

Swift B, Pfeifer ND, and Brouwer KLR (2010) Sandwich-cultured hepatocytes: an in vitro model to evaluate hepatobiliary transporter-based drug interactions and hepatotoxicity. *Drug Metab Rev* **42**:446–471.

Tchaparian EH, Houghton JS, Uyeda C, Grillo MP, and Jin L (2011) Effect of culture time on the basal expression levels of drug transporters in sandwich-cultured primary rat hepatocytes. *Drug Metab Dispos* **39**:2387–2394.

Trauner M, Wagner M, Fickert P, and Zollner G (2005) Molecular regulation of hepatobiliary transport systems: clinical implications for understanding and treating cholestasis. *J Clin Gastroenterol* **39**(4, Suppl 2):S111–S124.

Watanabe N, Tsukada N, Smith CR, and Phillips MJ (1991) Motility of bile canaliculi in the living animal: implications for bile flow. *J Cell Biol* **113**:1069–1080.

Watkins PB and Seeff LB (2006) Drug-induced liver injury: summary of a single topic clinical research conference. *Hepatology* **43**:618–631.

Zamek-Gliszczynski MJ, Kalvass JC, Pollack GM, and Brouwer KLR (2009) Relationship between drug/metabolite exposure and impairment of excretory transport function. *Drug Metab Dispos* **37**:386–390.

Zollner G, Wagner M, Fickert P, Silbert D, Gumhold J, Zatloukal K, Denk H, and Trauner M (2007) Expression of bile acid synthesis and detoxification enzymes and the alternative bile acid efflux pump MRP4 in patients with primary biliary cirrhosis. *Liver Int* **27**:920–929.

Address correspondence to: Kim L. R. Brouwer, UNC Eshelman School of Pharmacy, University of North Carolina at Chapel Hill, CB #7569, Chapel Hill, NC 27599-7569. E-mail: kbrouwer@email.unc.edu